

A Machine Learning Approach for Analyzing Texture and Morphometry Markers of Glioblastoma *TERT* Promoter Mutations in DAPI Fluorescence Images

Fatemeh Afsari^a, Ahmed Naglah^a, Akshita Gupta^b, Harshit Lohaana^c, Ugoma Onubogu^d,
Michalina Janiszewska^d, and Pinaki Sarder^a

^aDivision of Nephrology, Hypertension, and Renal Transplantation—Quantitative Health Section, Department of Medicine, College of Medicine, University of Florida, Gainesville, Florida, 32603, USA

^bDepartment of Health Outcomes and Biomedical Informatics, College of Medicine, University of Florida, Gainesville, Florida 32611, USA

^cDepartment of Computer and Information Science and Engineering, University of Florida, Gainesville, Florida 32611, USA

^dDepartment of Molecular Medicine, The Herbert Wertheim UF Scripps Institute for Biomedical Innovation and Technology, Jupiter, Florida, 33458, USA

ABSTRACT

Advanced molecular and imaging techniques, such as STAR-FISH, are frequently required to identify mutations in tissue specimens to properly diagnose Glioblastoma (GBM), an aggressive type of brain tumor. Mutations to the telomerase reverse transcriptase promoter (*TERT*_p) are common in cancer and present in approximately 80% of all GBM tumors. We hypothesize that machine learning can stratify cells by their *TERT*_p mutation status using DAPI fluorescence images since the STAR-FISH technique can be costly and inaccessible for some healthcare facilities.

In this study, we present a machine learning-based approach to recognize nuclei harboring *TERT*_p mutations solely based on the DAPI fluorescence images of GBM tissues. The proposed pipeline integrates a convolutional neural network (CNN)-based deep learning model to segment cells, extract hand-engineered features, and feed them into fully connected (FC) layers within the neural network or other machine learning classifiers to identify *TERT*_p mutant cells. This approach involves extracting DAPI features, including both morphological and textural image features, followed by an ensemble of machine learning modules to predict *TERT*_p mutant cells.

We evaluate our approach on a cohort of 18 patients (70 pairs of DAPI and STAR-FISH processed images). Our experimental results show that the FC layers within the neural network achieve the highest AUC, F1-Score, and recall of 0.77, 0.69, and 0.86, respectively, with the integrated CNN model achieving a Dice score of 0.83, accurately segmenting cells. Our work is one of the earliest attempts that we are aware of to use machine-learning models for *TERT*_p mutation identification using DAPI fluorescence images. Our results indicate the possibility of improved GBM diagnosis accuracy. To improve patient diagnosis and treatment planning for GBM, future research aims will expand the cohort and enhance the models to provide more precise and diagnostically valuable models for the interpretation of brain tissue.

Keywords: Glioblastoma, *TERT*_p Mutation, Machine Learning, Deep Learning, Nuclei Segmentation, Nuclei Classification, DAPI Fluorescence Images

Send correspondence to: Pinaki Sarder, PhD; Email - pinaki.sarder@medicine.ufl.edu

1. INTRODUCTION

GBM is the most aggressive and incurable brain tumor. Improvements in patient outcomes and treatment remain challenging despite progress in our understanding of the biology of these malignancies, with a median survival of approximately 16 months and a 5-year survival of 6.8%.¹ STAR-FISH (Specific to Allele PCR-FISH) combines *in situ* PCR and *in situ* fluorescence hybridization (FISH), which allows the simultaneous detection of point mutations and copy number variation at the single-cell level in intact formalin-fixed paraffin-embedded (FFPE) tissue samples.² Mutations to the telomerase reverse transcriptase promoter (*TERT*p) are common in cancer, present in approximately 80% of all GBM tumors³ and can be detected by STAR-FISH analysis. The *TERT*p is a highly structured genomic region that forms a G-quadruplex secondary structure.^{4,5} Recurrent mutations in this promoter alter the formation of this structure, resulting in chromatin structure remodeling.⁵ Since these changes likely impact broader chromatin organization, we hypothesize that machine learning algorithms can stratify cells according to *TERT*p mutation status based on nuclei features detected in DAPI fluorescence images. Therefore, the proposed approach can contribute to eliminating the need for a costly and time-consuming STAR-FISH protocol for detecting *TERT*p mutations, allow conducting other inexpensive imaging in conjunction with DAPI, such as histology imaging, and thus will offer rich data for further multi-modal analysis.

To test our hypothesis, we implement two categories of machine learning models: (a) models that rely on hand-engineered nuclei features and (b) models that automatically extract nuclei features using deep learning. In both approaches, the nuclei region is segmented using a CNN-based deep learning model. In the first category, we extract nuclei morphometry and texture features and train a classifier on these hand-engineered features to predict *TERT*p mutant cells. In the second category, we utilize a deep convolutional neural network (CNN) model⁶ that simultaneously performs segmentation and classification in a single step, producing detected cell instances with binary labels indicating *TERT*p mutant or non-mutated cells. To address the class imbalance, we apply a mitigation strategy by assigning higher weights to positive samples (*TERT*p mutant).

In this study, we make two key contributions: 1) We propose a novel pipeline for diagnosing GBM using only DAPI images, and 2) we provide a comparative analysis of two distinct machine learning approaches, hand-engineered feature-based models and deep learning-based models, for detecting *TERT*p mutations through nuclei texture and morphometry. The proposed pipeline can enable early diagnosis of GBM, contribute to understanding the chromatin structure remodeling in nuclei associated with *TERT*p, and contribute towards improved and more personalized GBM cancer management.

2. METHODOLOGY

In this section, we outline the methodology for *TERT*p mutation detection using DAPI images. Our pipeline begins with a CNN-based encoder-decoder model that performs simultaneous nuclei segmentation and classification. Following this, the segmented nuclei are used in a second approach where morphological and textural features are extracted and forwarded to the machine learning classifiers. Finally, we propose improvements to the encoder-decoder-based CNN architecture to enhance segmentation and classification accuracy. Each component of the pipeline is detailed in the following subsections.

2.1 CNN-Based Encoder-Decoder Model for Simultaneous Segmentation and Classification

The core component of our pipeline is a CNN-based encoder-decoder model, HoVerNet,⁶ which performs simultaneous nuclei segmentation and classification. HoVerNet has a single encoder for extracting image features and three decoder branches: one for segmenting nuclear objects, one for classifying nuclei types (e.g., *TERT*p mutant vs. non-mutant cells), and one for estimating spatial distances in the x and y directions to handle overlapping nuclei. This model achieves accurate segmentation, enabling the pipeline to detect nuclei instances effectively. However, its classification capability, particularly for DAPI images, proved to be suboptimal. While the segmentation branch excels at identifying individual nuclei across various image types, the classifier's performance on DAPI-stained samples was notably weak, indicating a need for significant improvements in this aspect of the model. The overall architecture of the HoVerNet model is depicted in Fig. 1.

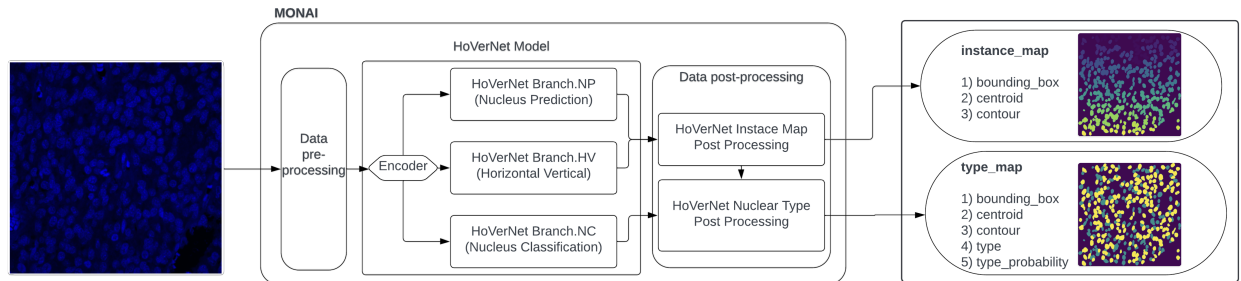


Figure 1: **Overall architecture of the HoVerNet model.** The model simultaneously segments nuclei, classifies cell types, and detects boundaries, enabling precise morphological analysis in histopathological images.

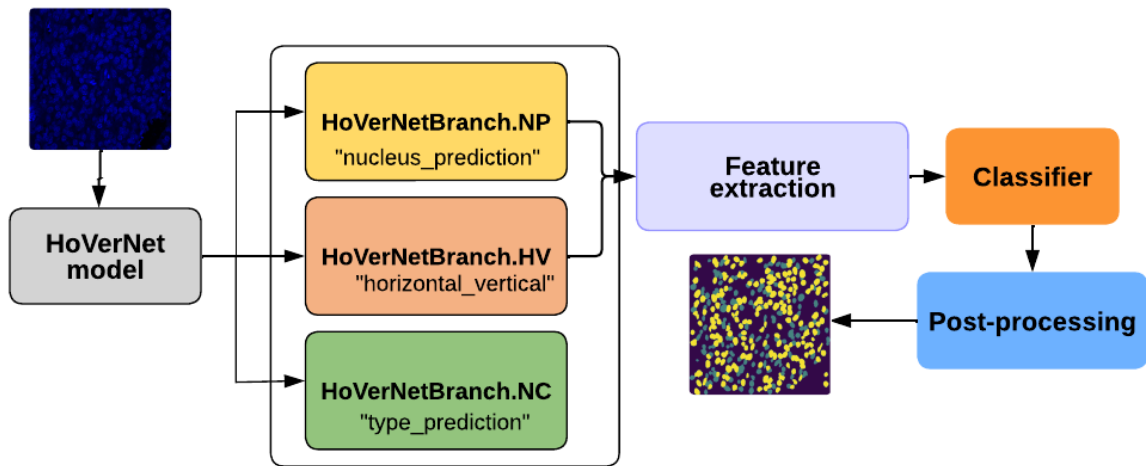


Figure 2: **Overview of the proposed computational pipeline utilizing the HoVerNet model.** Following cell contour segmentation, textural and morphological features are extracted from DAPI-stained images. A classification model is subsequently trained to accurately predict cell phenotypes. Finally, a post-processing step reconstructs the detected cells into a mask that preserves the spatial dimensions of the original image

2.2 Morphological and Textural Feature Extraction with Machine Learning Classifiers

To address the classification limitation of the HoVerNet model, the pipeline implements two additional steps following the initial segmentation where cell contours are detected. First, a feature extraction step is performed on the segmented nuclei. The feature extraction procedure extracts hand-engineered morphological features, such as cell size, shape, and boundary characteristics, and textural features, such as intensity patterns and variations, from the segmented nuclei. A separate classifier training phase follows this step. The proposed pipeline is depicted in Fig. 2. Machine learning classifiers include fully connected layers within an artificial neural network (ANN), support vector machine (SVM), random forest (RF), and logistic regression (LR). The ANN consists of three dense hidden layers (sizes 16, 8, and 8) and a single output layer of size 1. It is optimized using Stochastic Gradient Descent (SGD) with a learning rate of 0.0001. In comparison, the SVM employs a sigmoid kernel, and the RF model uses 1000 trees with a maximum depth of 10. These post-segmentation steps are designed to enhance the model's ability to accurately classify nuclei, particularly in DAPI images, by exploiting the information from the well-performing segmentation branch.

2.3 Improvements to the Encoder-Decoder-Based CNN Architecture

Finally, we propose enhancements to the encoder-decoder-based CNN architecture to improve segmentation and classification accuracy. While HoVerNet performs well on PAS and H&E stained histology images, it struggles

to classify *TERT*p mutant versus non-mutant cells in DAPI fluorescence images. To address this limitation, we introduce HoVerNet+, an extension of HoVerNet tailored for DAPI images.

HoVerNet+ replaces the pixel-level Dice and cross-entropy loss functions with an object-level Intersection over Union (IoU)-based loss function, which better captures whole-cell characteristics. The loss function is defined as:

$$\mathcal{L} = 1 - \sum_{c=1}^C \frac{1}{N_c} \sum_{i=1}^{N_c} \frac{|G_{c,i} \cap P_{c,i}|}{|G_{c,i} \cup P_{c,i}|}, \quad (1)$$

where c and C denote the class index and total number of classes, N_c is the number of objects in the ground truth class c , and $G_{c,i}$ and $P_{c,i}$ are the i -th ground truth and predicted objects, respectively.

Additionally, we apply class weights to penalize misclassified samples, mitigating the effects of class imbalance in the dataset. These improvements enhance the ability of the model to classify *TERT*p mutant cells and segment nuclei accurately in DAPI images.

3. DATA

Data has been collected from 18 patients, each contributing one tissue sample. Tissue specimens have been prepared, processed, and scanned into DAPI fluorescence images. This process yielded a total of 70 DAPI fluorescence digital images that were used for analysis, indicating that we obtained more than one image from some patients. To generate the ground truth labels, we utilized fluorescence images of intact GBM tissue processed using STAR-FISH to identify cells with *TERT*p mutations.² This *in situ* PCR-based method allows the detection of single nucleotide alterations at the single-cell level and has previously been validated for *TERT*p mutations.^{7,8} Briefly, mutation-specific PCR is performed *in situ*, and the presence of the amplicon is detected by *in situ* hybridization of a fluorescence-labeled probe using confocal microscopy. The images are exported in the form of high-quality TIFF files. From the ground truth label images, we extract two masks: the cell object mask and the cell type mask. The cell object mask identifies and delineates individual cellular instances, while the cell type mask classifies the types of cells or structures as *TERT*p mutant or non-mutated within each instance. To summarize, our dataset comprises: *a) DAPI fluorescence images*: DAPI fluorescence images are cropped to a standardized dimension of 800×800 pixels per image, ensuring uniformity in analysis across all samples. This cropping step standardizes the input size while preserving the original spatial resolution of the images. *b) Instance Maps*: A *TERT*p STAR-FISH processed and registered signal image, regardless of the cell type, with a size of 800×800 pixels, serves as the cell object mask for each DAPI fluorescence image. *c) Type Maps*: A cell type mask specifies two classes: the *TERT*p mutant class and the non-mutated class. This mask outlines the nuclei classification procedure using the previously reported STAR-FISH processed signal,⁸ which enables specific biological assessments and comparisons throughout the dataset.

4. RESULTS

We implemented and tested the proposed pipeline on our dataset ($N = 70$). The images, consisting of registered DAPI and STAR-FISH sections, were divided into 70% training, 15% validation, and 15% testing sets, ensuring stratified splits such that all images from each patient were allocated to only one set. The training set includes 1225 overlapping patches of size 540×540 pixels, while the validation and the testing sets contain 175 patches each. The CNN model was trained using the DAPI images as input and the STAR-FISH signal images as ground truth labels for *TERT*p mutant cell detection.

Our experimental findings demonstrate that our proposed machine learning-based method was effective in identifying morphometric and textural features in DAPI images that can distinguish between *TERT*p mutants and non-mutated cells. Table 1 shows that the proposed pipeline can achieve AUC, F1-score, precision, and recall of 0.77, 0.69, 0.58, and 0.86, respectively, using the ANN method. Fig. 3 shows that the proposed pipeline can achieve $\text{AUC} > 0.5$ (random guess baseline) using all methods, which implies that the nuclei textures present in DAPI images may contain information about the chromatin structure remodeling associated with mutations to

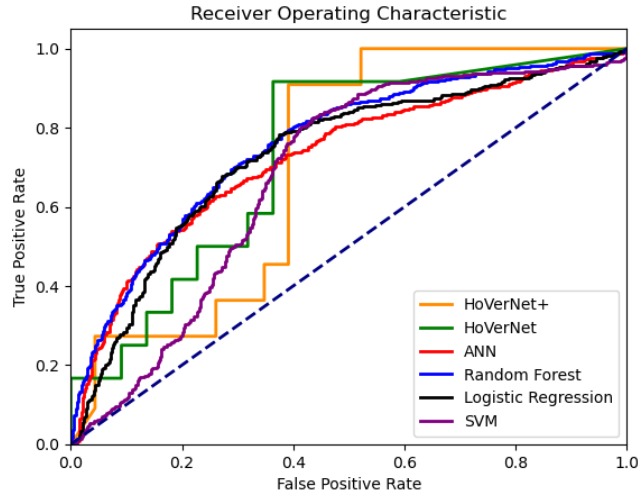


Figure 3: **ROC curves of the proposed modules.** The curves illustrate the predictive performance of each module, depicting the trade-off between sensitivity and specificity across different classification thresholds.

Table 1: **AUC-ROC results of the proposed machine learning modules and HoVerNet.**⁶ The table presents the classification performance of each model, with the highest values in each column highlighted in bold.

Features	Model	AUC	F1 Score	Precision	Recall
Automated	HoVerNet+	0.71	0.61	0.72	0.53
	HoVerNet ⁶	0.73	0.61	0.75	0.52
Hand-engineered	Logistic Regression	0.73	0.56	0.82	0.42
	Random Forest	0.77	0.60	0.84	0.47
	Support Vector Machine	0.67	0.62	0.86	0.48
	ANN	0.77	0.69	0.58	0.86

TERTp. Therefore, we suggest that machine learning can be used for analyzing DAPI images to enable fast and early detection of GBM in cases where the STAR-FISH technology is not available.

Our analysis suggests that both model categories (hand-engineered versus automated-extracted deep features) can achieve comparable results. However, we can observe that hand-engineered features can achieve better performance. Table 1 shows that the hand-engineered features achieved AUC, F1-score, precision, and recall of up to 0.77, 0.69, 0.86, and 0.86, respectively, compared to the automated features that achieved AUC, F1-score, precision, and recall of up to 0.73, 0.61, 0.75, and 0.53, respectively. Our results suggest that hand-engineered features can perform better biological representation of tissue and can minimize the effect of noise patterns that may have a negative influence on feature extraction using deep learning.

To further assess the performance of the pipeline, we evaluated the percentage of *TERTp* mutated cells detected per patient and compared it to the ground truth obtained from STAR-FISH analysis. Across the testing set, the proposed method identified an average of 59.74% of mutated cells per patient, closely aligning with the ground truth percentage of 40.66% (standard deviation 10.93%). A correlation analysis revealed a moderate to strong agreement between the predicted and ground truth percentages, with a Pearson correlation coefficient of $r = 0.67$, indicating that the model reliably detects mutated cells across diverse patient samples. Additionally, a Bland-Altman plot was depicted in Fig. 4 to assess the agreement between the model predictions and the ground truth. While the Bland-Altman analysis shows a moderate agreement with the ground truth, with a mean bias of 19.08%, suggesting a slight underestimation of the predictions, the limits of agreement (LOA) ranging from 13.64% to 51.80% indicate some variability in the model's predictions. This variability suggests potential areas for improvement, and future work could focus on refining the model to achieve more consistent performance, particularly in minimizing bias and reducing the range of LOA. However, this analysis further confirms that the variation in detection accuracy remained within clinically acceptable ranges, underscoring the robustness and

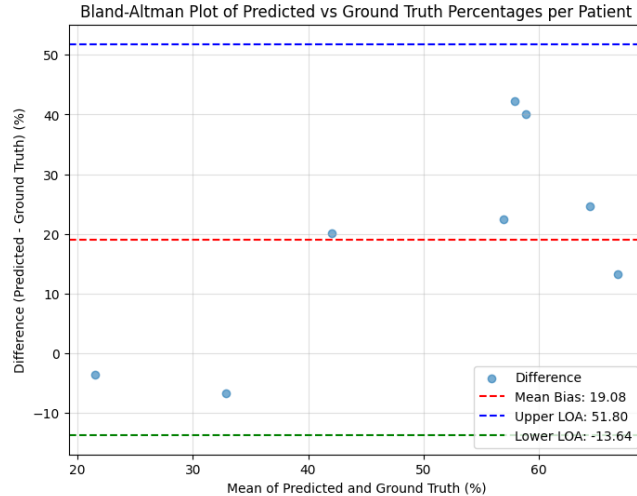


Figure 4: **Bland-Altman plot showing the agreement between the predicted and ground truth percentages of *TERTp*-mutated cells across patients.** The x-axis represents the mean of the predicted and ground truth percentages, while the y-axis represents the difference (predicted minus ground truth).

generalizability of the proposed approach in quantifying *TERTp* mutations across diverse patient samples.

5. CONCLUSION

This paper presented a machine-learning approach for classifying *TERTp* mutant cells and segmenting the cells in GBM tissue images. Our proposed pipeline incorporated an ensemble of deep CNN modules and machine-learning classification based on both hand-engineered and automated features. We proposed a novel ANN model, along with SVM, RF, and LR classification models, as well as a deep CNN with a task-specific loss function. The experimental results demonstrated that nuclei features in DAPI fluorescence images can provide essential information. Moreover, our findings indicated that, while the deep CNN model could successfully segment nuclei, it had limitations in accurately identifying nuclei types, particularly discriminating between *TERTp* mutant and non-mutated cells in the DAPI images, which we anticipated would improve by expanding the sample size. Alternatively, the classification performance of ANN was the highest, indicating that its feature set may be included in the deep CNN to improve the classification performance. We plan to expand on the results of this work by addressing these areas to produce more accurate and clinically useful models for the interpretation of images of GBM tissue on the expanded cohort of patients. This future work will ultimately help improve patient diagnosis and treatment planning for GBM patients.

ACKNOWLEDGMENTS

This work was supported by the American Cancer Society University of Florida Institutional Grant (MJ & PS). All experiments with the use of human tumor tissue were approved by Scripps Research IRB protocol #IRB-18-7209.

REFERENCES

- [1] Wen, P. Y., Weller, M., Lee, E. Q., Alexander, B. M., Barnholtz-Sloan, J. S., Barthel, F. P., Batchelor, T. T., Bindra, R. S., Chang, S. M., Chiocca, E. A., et al., “Glioblastoma in adults: a society for neuro-oncology (sno) and european society of neuro-oncology (eano) consensus review on current management and future directions,” *Neuro-oncology* **22**(8), 1073–1113 (2020).
- [2] Janiszewska, M., Liu, L., Almendro, V., Kuang, Y., Paweletz, C., Sakr, R. A., Weigelt, B., Hanker, A. B., Chandarlapaty, S., King, T. A., et al., “In situ single-cell analysis identifies heterogeneity for pik3ca mutation and her2 amplification in her2-positive breast cancer,” *Nature genetics* **47**(10), 1212–1219 (2015).

- [3] Tarabichi, M., Demeulemeester, J., Verfaillie, A., Flanagan, A. M., Loo, P. V., and Konopka, T., “A pan-cancer landscape of somatic substitutions in non-unique regions of the human genome,” *bioRxiv*, 2020–04 (2020).
- [4] Patel, D. J., Phan, A. T., and Kuryavyi, V., “Human telomere, oncogenic promoter and 5-utr g-quadruplexes: diverse higher order dna and rna targets for cancer therapeutics,” *Nucleic acids research* **35**(22), 7429–7455 (2007).
- [5] Mukherjee, A. K., Sharma, S., and Chowdhury, S., “Non-duplex g-quadruplex structures emerge as mediators of epigenetic modifications,” *Trends in Genetics* **35**(2), 129–144 (2019).
- [6] Graham, S., Vu, Q. D., Raza, S. E. A., Azam, A., Tsang, Y. W., Kwak, J. T., and Rajpoot, N., “Hovernet: Simultaneous segmentation and classification of nuclei in multi-tissue histology images,” *Medical image analysis* **58**, 101563 (2019).
- [7] Walentynowicz, K. A., Engelhardt, D., Cristea, S., Yadav, S., Onubogu, U., Salatino, R., Maerken, M., Vincentelli, C., Jhaveri, A., Geisberg, J., et al., “Single-cell heterogeneity of egfr and cdk4 co-amplification is linked to immune infiltration in glioblastoma,” *Cell reports* **42**(3) (2023).
- [8] Onubogu, U., Gatenbee, C. D., Prabhakaran, S., Wolfe, K. L., Oakes, B., Salatino, R., Vaubel, R., Szentirmai, O., Anderson, A. R., and Janiszewska, M., “Spatial analysis of recurrent glioblastoma reveals perivascular niche organization,” *JCI insight* **9**(12) (2024).